Electronic Supplementary Information

Influence of the surface terminal groups on the efficiency of two-electron oxygen reduction reaction by iron single atoms on $Ti_3C_2T_x$ (T_x=Cl, Br, NH) MXene

Dawid Daniël Kruger,[a] Juan José Delgado,[b] F. Javier Recio,*[c] Sara Governa-Ferron,[a] Ana Primo *[a] and Hermenegildo García *[a]

a. *Instituto Universitario de Tecnología Química CSIC-UPV, Universitat Politècnica de València, Av. De los Naranjos s/n, València, 46022, Spain.*
E-mail: aprimoar@itq.upv.es
E-mail: hgarcia@itq.upv.es

b. *Material Science and Metallurgy Engineering and Inorganic Chemistry, University of Cádiz, 11510 Puerto Real, Cádiz, Spain.*

c. *Departamento de Química Física Aplicada, Facultad de Ciencias, Universidad Autónoma de Madrid, C/Francisco Tomás y Valiente, 7, Cantoblanco, 28049 Madrid, Spain.*
E-mail: javier.recioc@uam.es

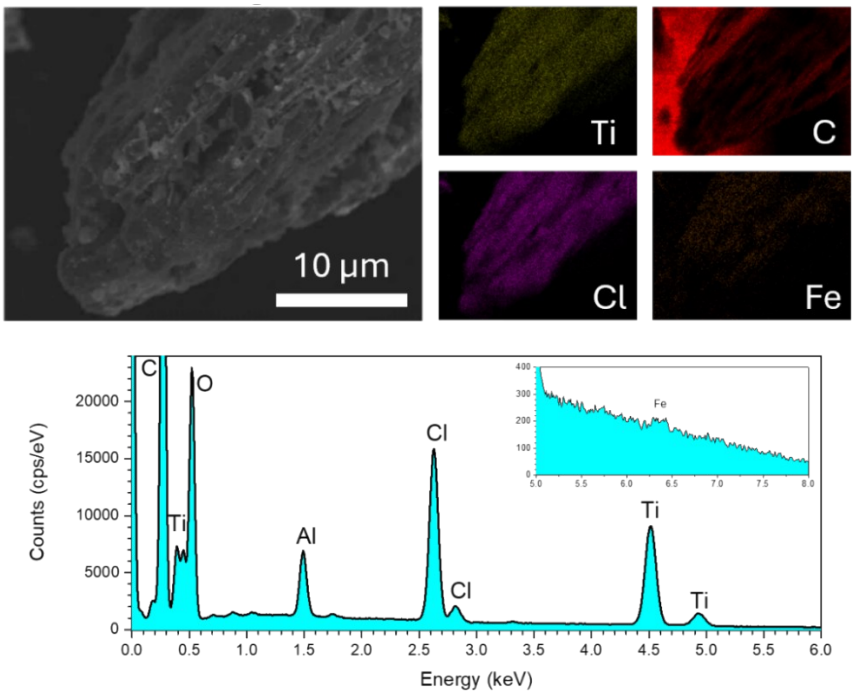

Figure S1 – SEM image of Fe(SA)-$Ti_3C_2Cl_x$ with corresponding EDS maps and spectrum.

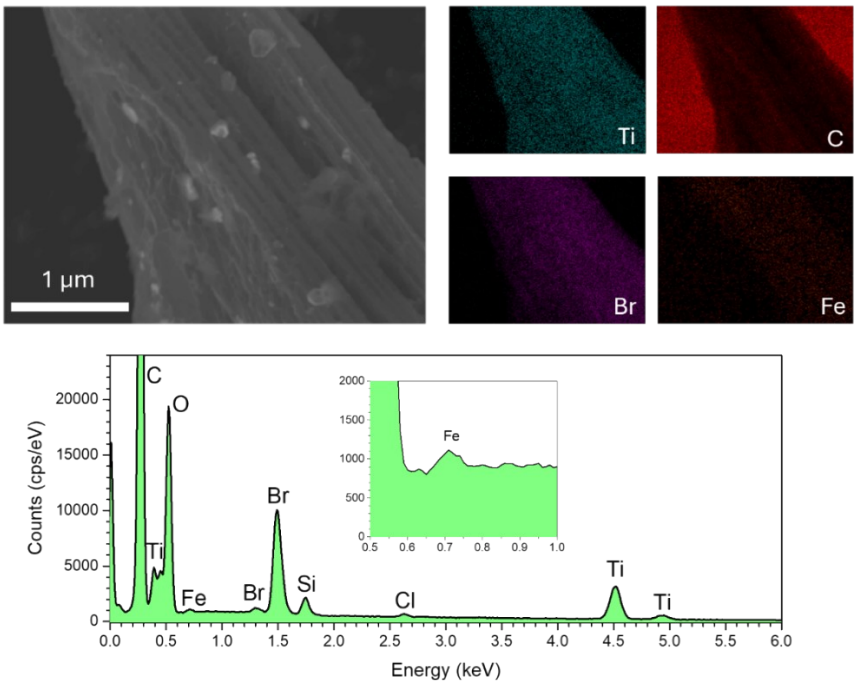

Figure S2 – SEM image of Fe(SA)-$Ti_3C_2Br_x$ with corresponding EDS maps and spectrum.

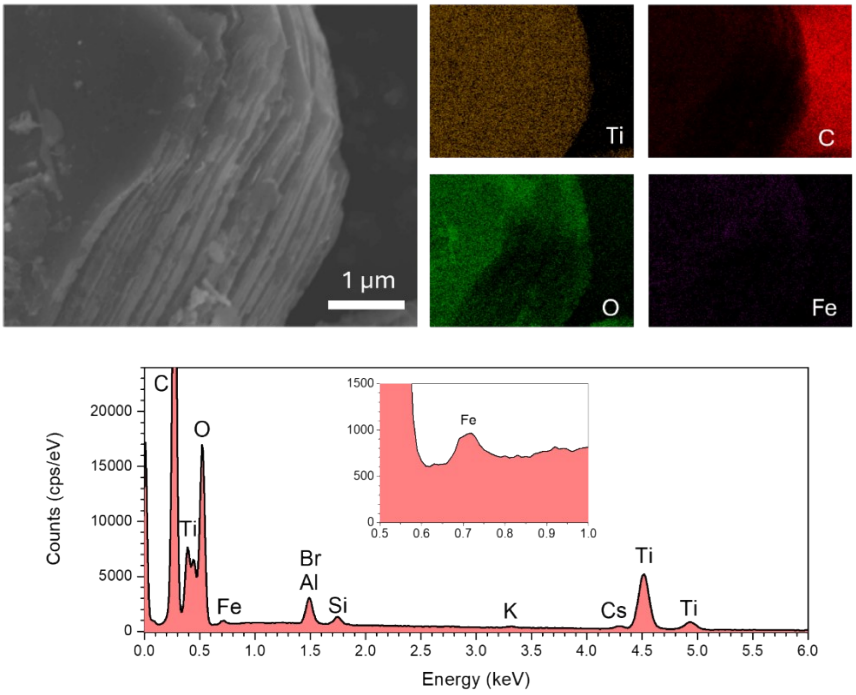

Figure S3 – SEM image of Fe(SA)-$Ti_3C_2(NH)_x$ with corresponding EDS maps and spectrum. Note that the main peak of the N KL transition (0.3924 keV) is masked by the more intense Ti $L_{III}M_I$ (0.3953 keV) and $L_{II}M_I$ (0.4013 keV) peaks.

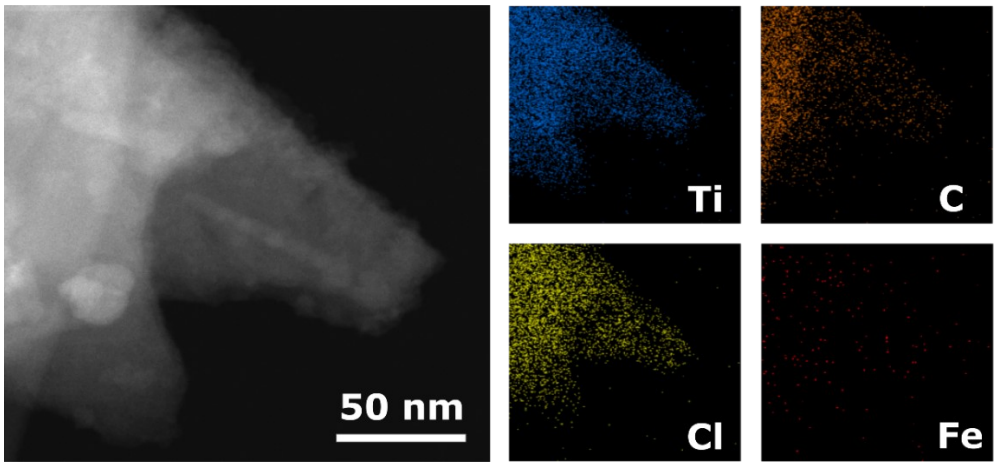

Figure S4– HAADF-STEM image of Fe(SA)-$Ti_3C_2Cl_x$ with corresponding EDX maps.

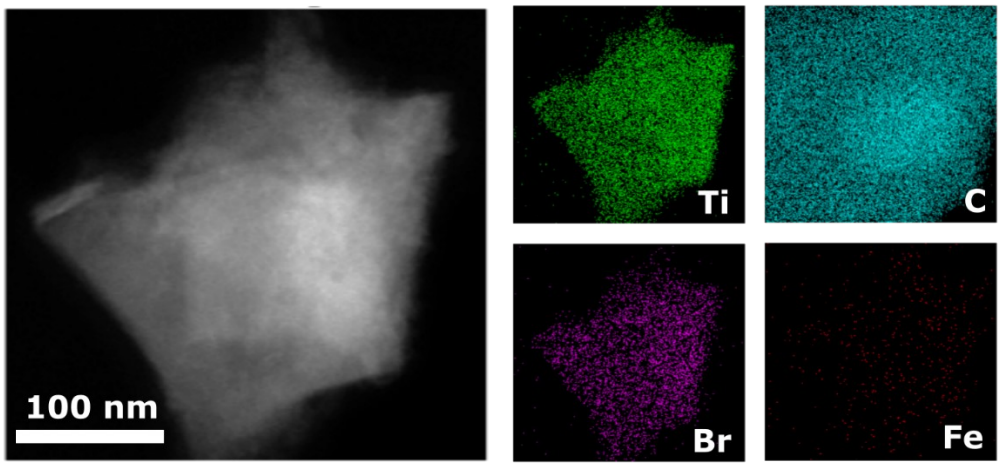

Figure S5– HAADF-STEM image of Fe(SA)-$Ti_3C_2Br_x$ with corresponding EDX maps

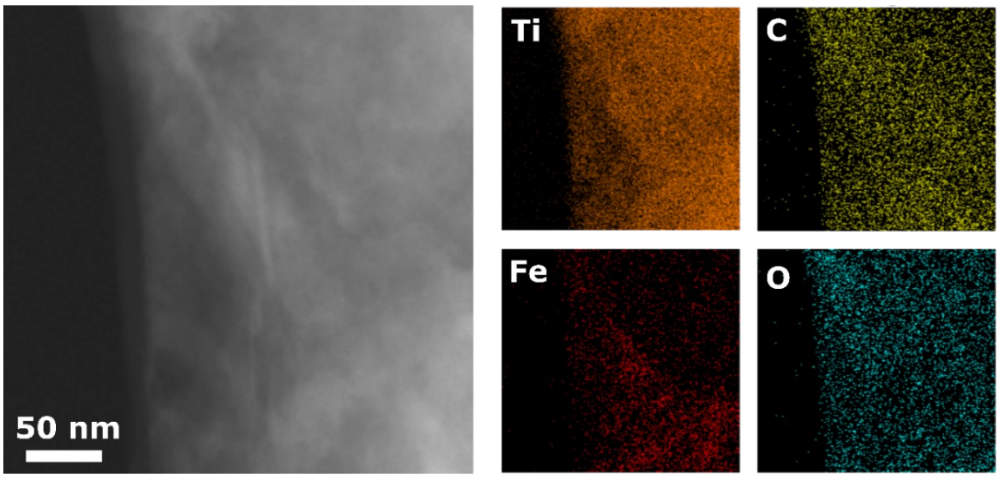

Figure S6– HAADF-STEM image of Fe(SA)-$Ti_3C_2(NH)_x$ with corresponding EDX maps.

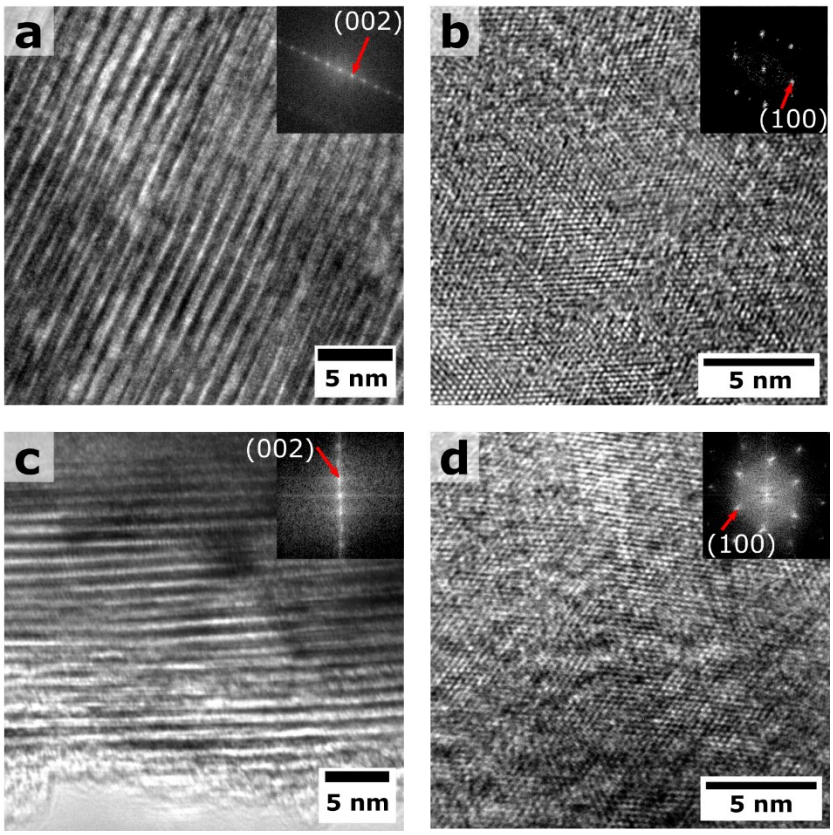

Figure S7 – High resolution transmission electron microscope images showing (a) Fe(SA)-$Ti_3C_2Cl_x$ as viewed perpendicular to the <001> zone axis, (b) Fe(SA)-$Ti_3C_2Cl_x$ as viewed along the <001> zone axis, (c) Fe(SA)-$Ti_3C_2Br_x$ as viewed perpendicular to the <001> zone axis, (d) Fe(SA)-$Ti_3C_2Br_x$ as viewed along the <001> zone axis, with insets showing the FFT patterns.

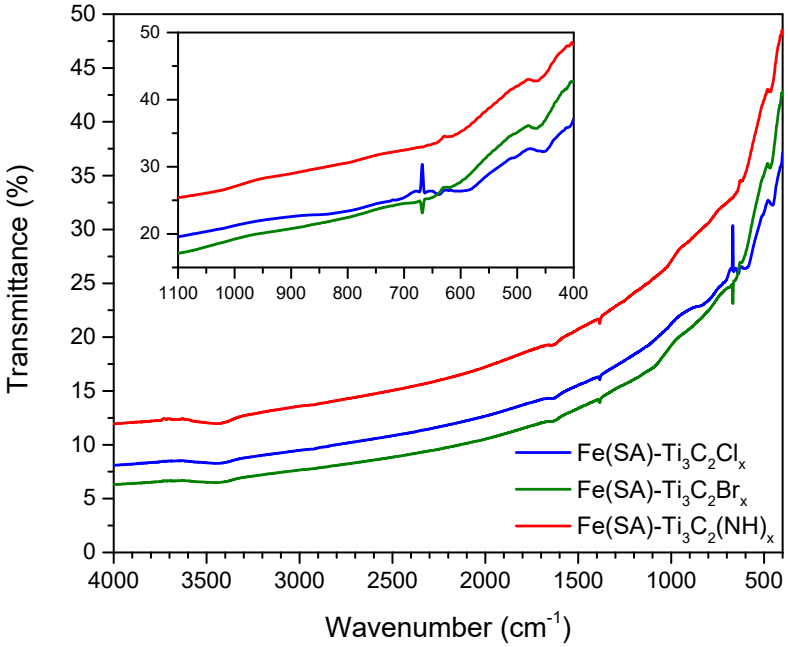

Figure S8 – ATR-FTIR spectra of the Fe(SA)-$Ti_3C_2T_x$ samples under study. The inset shows and expansion of the low frequency region showing the shift of the characteristic Ti-C skeletal vibration between 500 and 450 cm^{-1}.

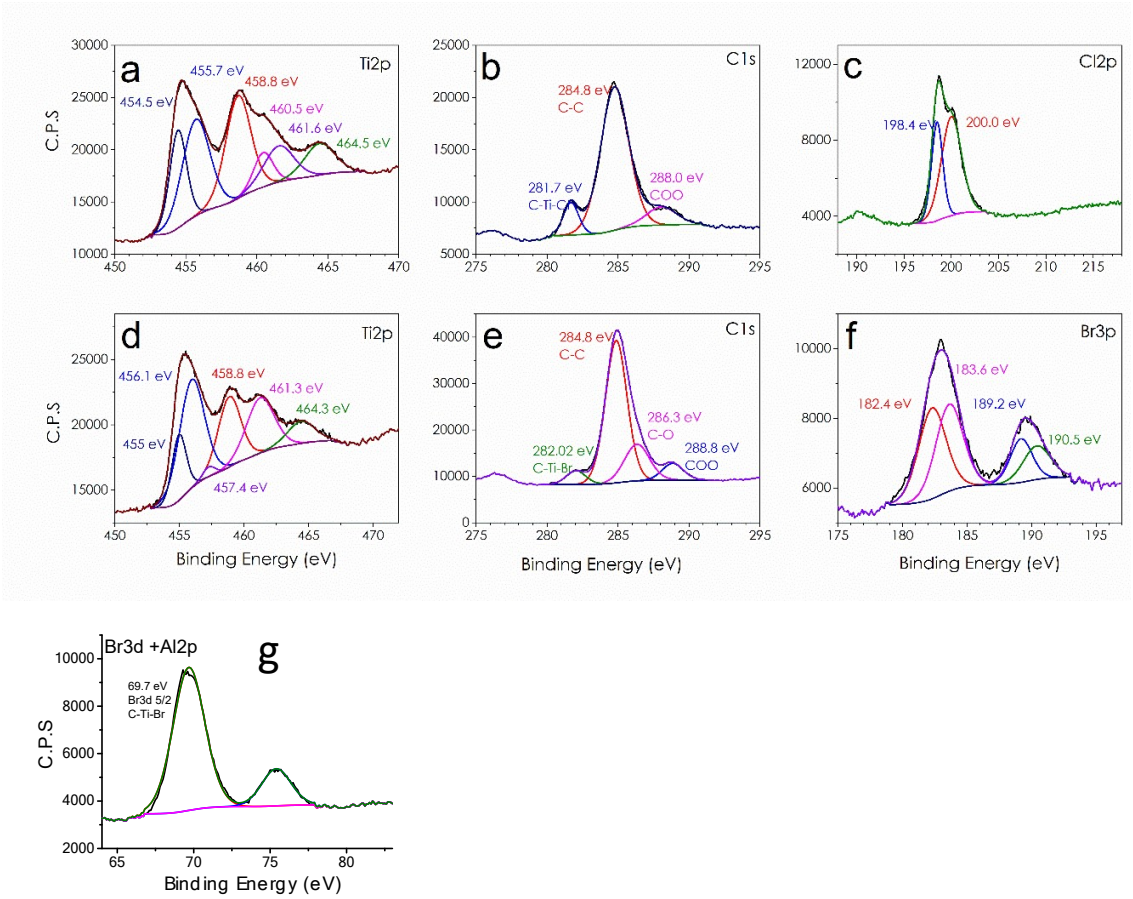

Figure S9 – High resolution XPS of (a) Ti 2p, (b) C 1s, and (c) Cl 2p levels of Fe(SA)-$Ti_3C_2Cl_2$, and (d) Ti 2p, (e) C 1s, (f) Br 3p and g) Br 3d and Al 2p levels of Fe(SA)-$Ti_3C_2Br_x$ MXene samples, with the corresponding deconvolution to individual components.

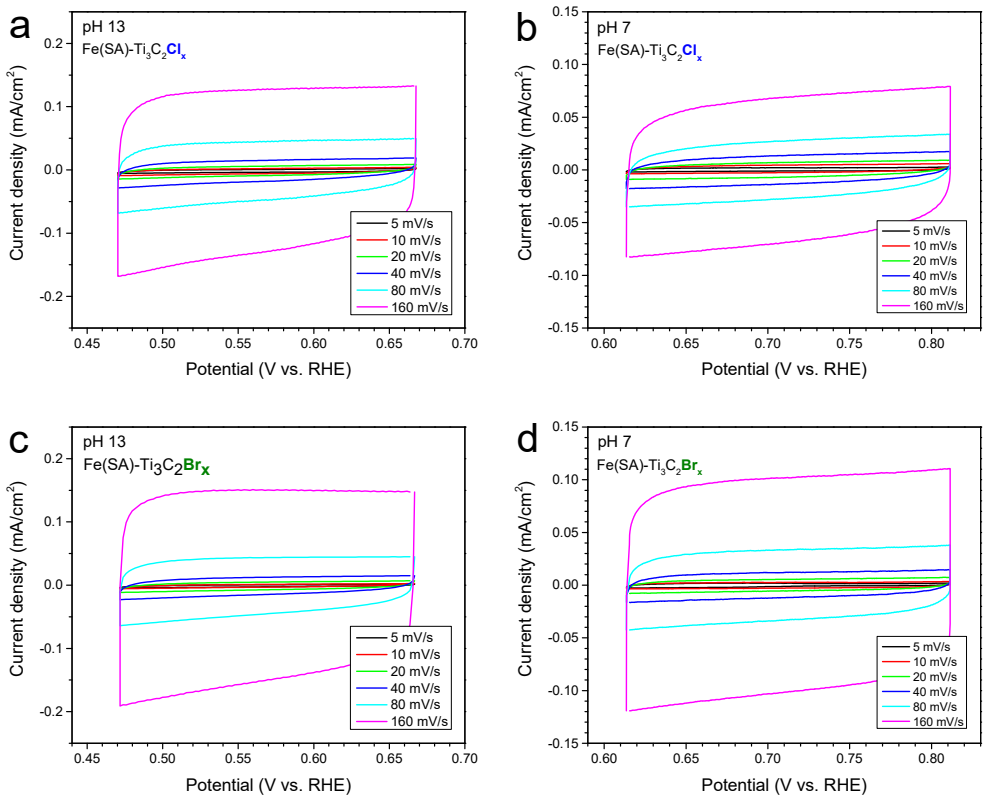

Figure S10 - Cyclic voltammetry curves of Fe(SA)-$Ti_3C_2Cl_2$ in N_2 purged (a) 0.1 M KOH, and, (b) 0.5 M Na_2SO_4 and Fe(SA)-$Ti_3C_2Br_x$ in N_2 purged (c) 0.1 M KOH, and (d) 0.5 M Na_2SO_4, at various scan rates to determine the double-layer capacitance (C_{dl}).

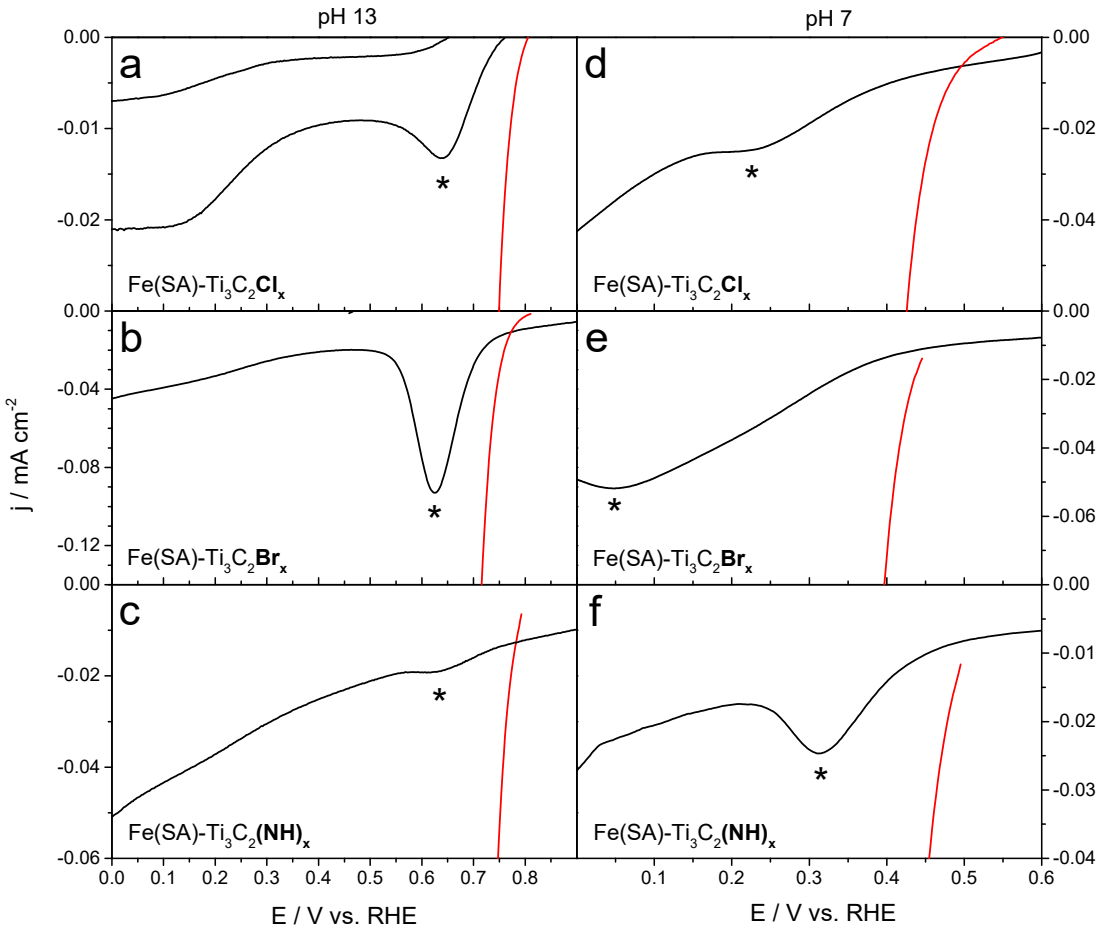

Figure S11 - Cyclic voltammetry curves in N_2 purged 0.1 M KOH of (a) of Fe(SA)-$Ti_3C_2Cl_x$, (b) Fe(SA)-$Ti_3C_2Br_x$, and (c) Fe(SA)-$Ti_3C_2(NH)_x$, and in N_2 purged 0.5 M Na_2SO_4 of (d) of Fe(SA)-$Ti_3C_2Cl_2$, (e) Fe(SA)-$Ti_3C_2Br_x$, and (f) Fe(SA)-$Ti_3C_2(NH)_x$, at a scan rate of 5 mV s^{-1}. Peaks likely associated with the reduction of Fe(iii) to Fe(ii) are indicated by asterisks symbols (*). The corresponding ORR kinetic currents after saturation with O_2 are shown in red.

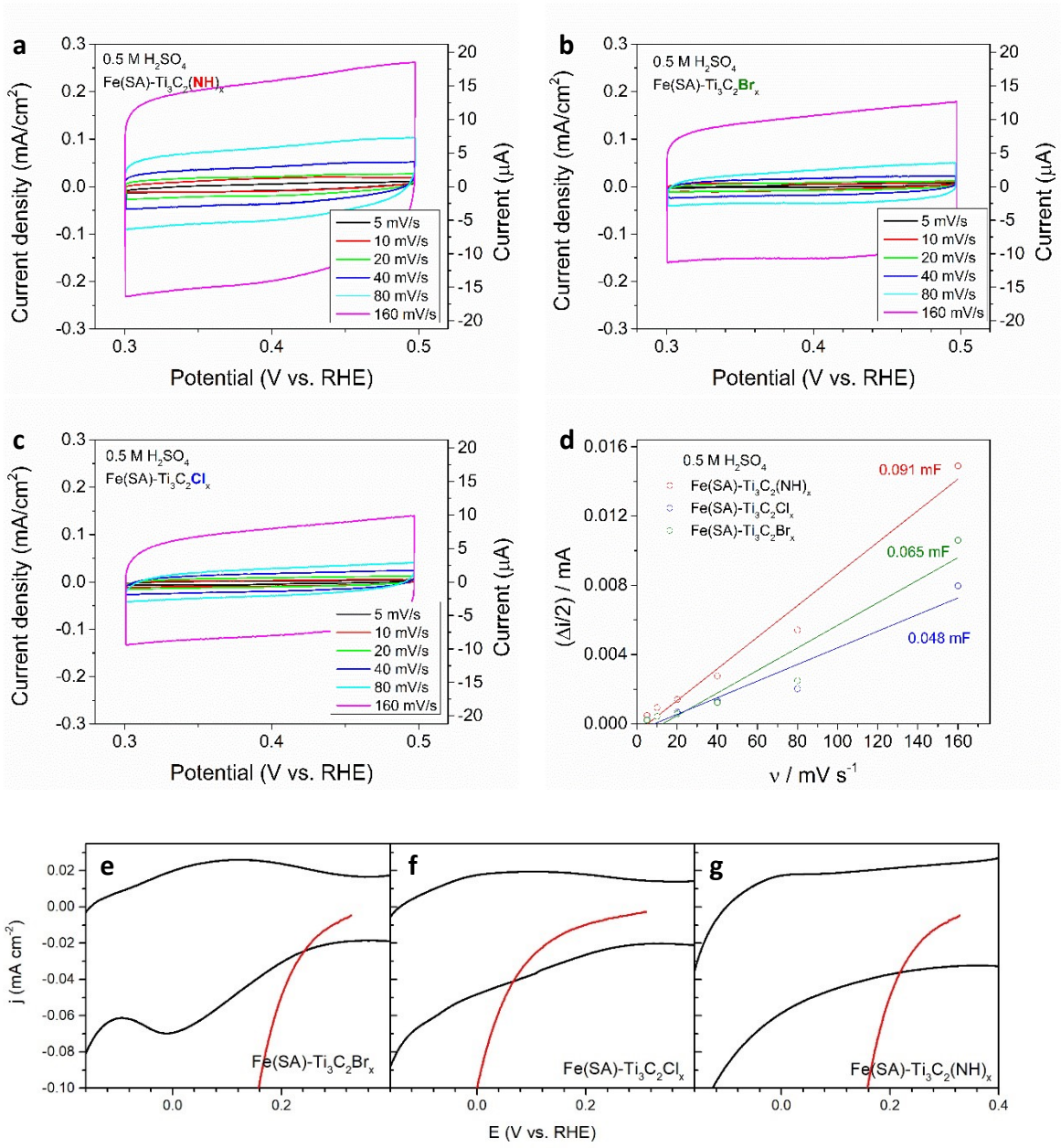

Figure S12 – (a-c) Cyclic voltammetry plots of Fe(SA)-$Ti_3C_2T_x$ (T=Cl, Br, NH) recorded at various scan rates in N_2 purged 0.5 M H_2SO_4. (d) C_{dl} determination from cyclic voltammetry measurements of Fe(SA)-$Ti_3C_2T_x$ samples. Cyclic voltammetry curves (black lines) at a scan rate of 5 mV s^{-1} in N_2 purged 0.5 M H_2SO_4 measured for (e) Fe(SA)-$Ti_3C_2Br_x$, (f) Fe(SA)-$Ti_3C_2Cl_x$, and (g) Fe(SA)-$Ti_3C_2(NH)_x$. The red lines in plots e-f show the corresponding ORR current measured for these electrodes under O_2-saturated electrolyte.

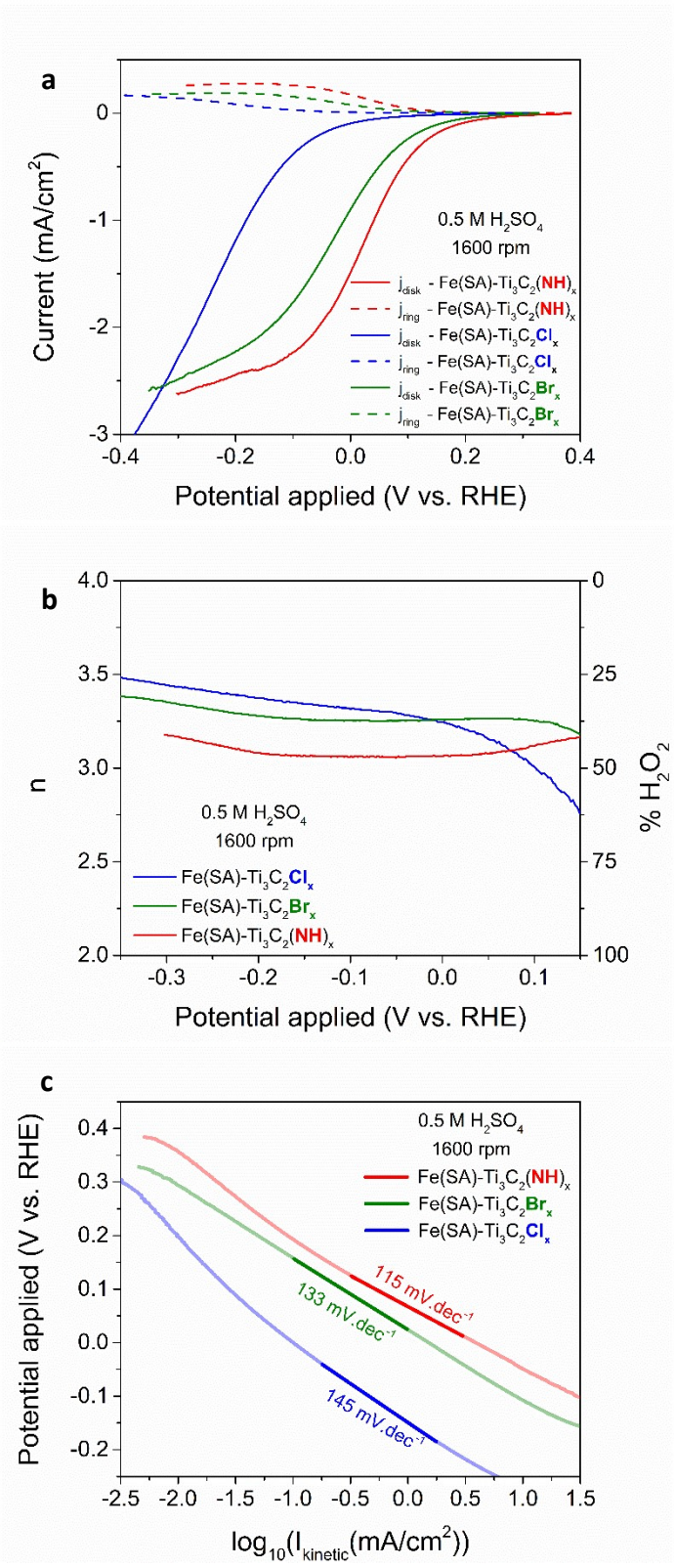

Figure S13 - (a) RRDE linear sweep voltammetry polarization curves recorded at 0.005 V s^{-1} of Fe(SA)-$Ti_3C_2T_x$ (T = Cl, Br, NH) in O_2 saturated 0.5 M H_2SO_4 electrolyte (normalised to disk area), with (b) corresponding electron transfer numbers, n, and H_2O_2 selectivity, and (c) Tafel slopes in the kinetic region.

Table S1 - Electrochemical characterization data in H_2SO_4 electrolyte of the $Ti_3C_2T_x$ (T = Cl, Br, NH) MXenes under study.

Catalyst	E_{onset} (V vs. RHE)	n e^{-} [a]	E_{red} (V vs. RHE)	C_{dl} (mF)	ECSA, ($m^2\ g^{-1}$)
0.5 M H_2SO_4					
Fe(SA)-$Ti_3C_2Cl_2$	-0.007	3.24	-	0.048	17.0
Fe(SA)-$Ti_3C_2Br_x$	0.167	3.26	-0.01	0.065	23.0
Fe(SA)-$Ti_3C_2(NH)_x$	0.181	3.07	-	0.091	32.2

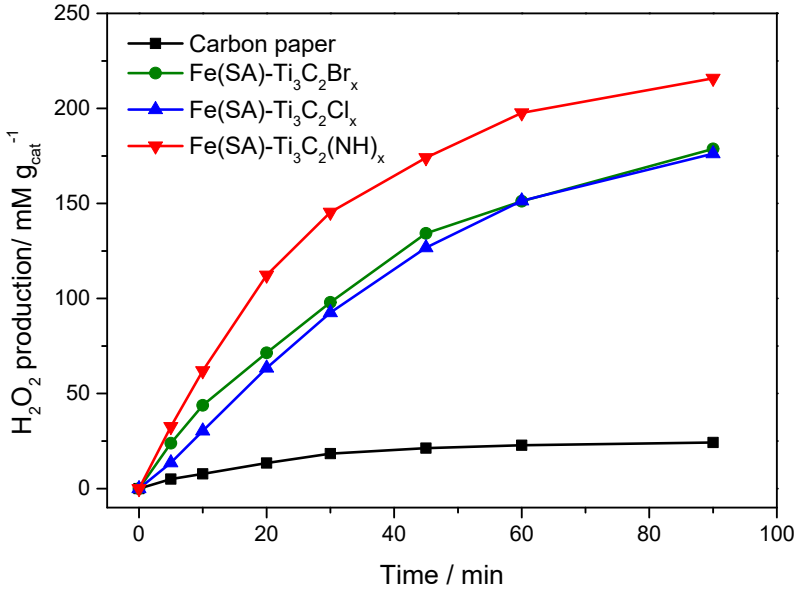

Figure S14 – Quantification of electrochemically produced H_2O_2 in 0.05 M Na_2SO_4 electrolyte in a prototype cell with Fe(SA)-$Ti_3C_2T_x$ electrocatalysts deposited onto carbon paper as air cathodes. Detection of H_2O_2 was determined by complexation with titanium (IV) oxysulfate and subsequent measurement of UV-Vis absorbance at 410 nm.

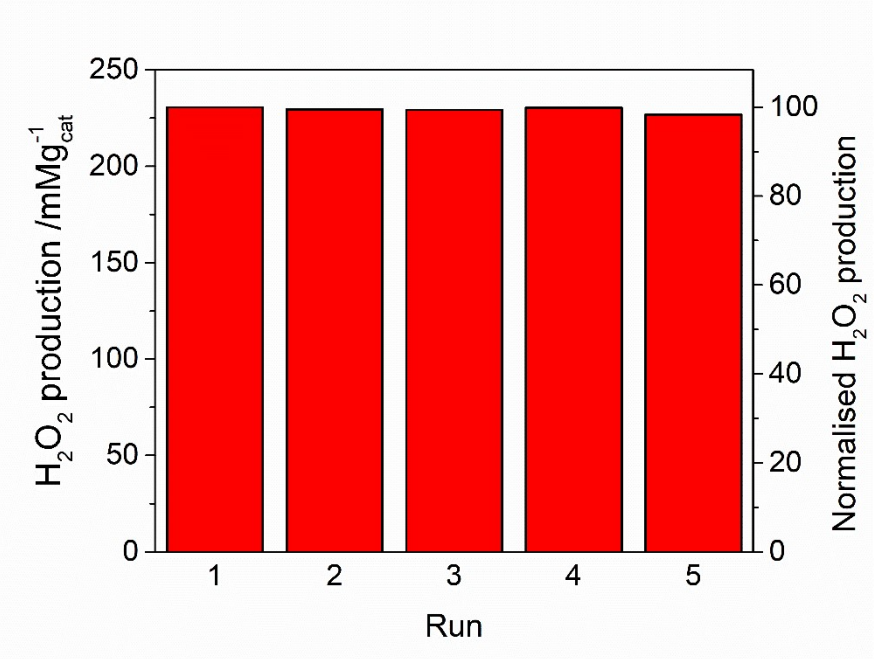

Figure S15 – Repeat electrochemical H_2O_2 generation tests for a Fe(SA)-$Ti_3C_2(NH)_x$ modified carbon paper air cathode in 0.05 M Na_2SO_4 electrolyte in a prototype cell. Detection of H_2O_2 was measured after 90 minutes for each repeat run.